LBL-30249
UC-407
Preprint

Lawrence Berkeley Laboratory

UNIVERSITY OF CALIFORNIA

ENERGY & ENVIRONMENT DIVISION

Submitted to Journal of Aerosol Science

Numerical Investigations of the Deposition of Unattached ^{218}Po and ^{212}Pb from Natural Convection Enclosure Flow

W.W. Nazaroff, D. Kong, and A.J. Gadgil

February 1992

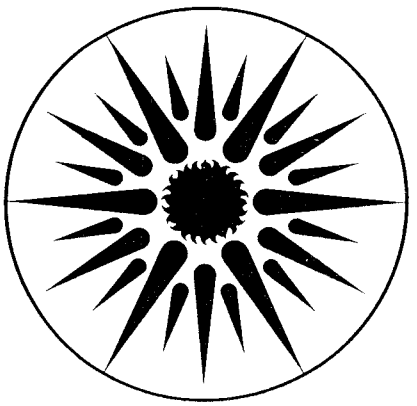

ENERGY & ENVIRONMENT DIVISION

Prepared for the U.S. Department of Energy under Contract Number DE-AC03-76SF00098

LBL-30249

Accepted for publication in *Journal of Aerosol Science*,
February, 1992.

Numerical Investigations of the Deposition of Unattached ^{218}Po and ^{212}Pb from Natural Convection Enclosure Flow

William W. Nazaroff,*† Dung Kong,* and Ashok J. Gadgil†

*Department of Civil Engineering
University of California
Berkeley, CA 94720 USA

†Indoor Environment Program
Energy and Environment Division
Lawrence Berkeley Laboratory
University of California
Berkeley, CA 94720 USA

February 1992

This work was supported in part by the Universitywide Energy Research Group of the University of California, and by the Director, Office of Energy Research, Office of Health and Environmental Research, Human Health and Assessments Division and Pollutant Characterization and Safety Research Division of the U.S. Department of Energy under Contract No. DE-AC03-76SF00098. Additional support was provided by a grant from the Berkeley Engineering Fund.

NUMERICAL INVESTIGATIONS OF THE DEPOSITION OF UNATTACHED ^{218}PO AND ^{212}PB FROM NATURAL CONVECTION ENCLOSURE FLOW

William W Nazaroff, Dung Kong and Ashok J. Gadgil

Abstract—We report numerical predictions of the deposition to enclosure surfaces of unattached ^{218}Po and ^{212}Pb, short-lived decay products of ^{222}Rn and ^{220}Rn, respectively. The simulations are conducted for square and rectangular two-dimensional enclosures under laminar natural convection flow with Grashof numbers in the range 7×10^7 to 8×10^{10}. The predictions are based upon a finite-difference natural-convection fluid-mechanics model that has been extended to simulate the behavior of indoor radon decay products. In the absence of airborne particles, the deposition velocity averaged over the enclosure surface was found to be in the range (2-4) $\times 10^{-4}$ m s^{-1} for ^{218}Po and (1-3) $\times 10^{-4}$ m s^{-1} for ^{212}Pb. In each simulation, the deposition rate varied by more than an order of magnitude around the surface of the enclosure with the largest rates occurring near corners. Attachment of decay products to airborne particles increased the deposition velocity; for example, attachment of ^{218}Po at a rate of 50 h^{-1} increased the predicted average deposition velocity by 30-70% over values in the absence of attachment. The simulation results have significance for assessing the health risk associated with indoor exposure to ^{222}Rn and ^{220}Rn decay products and for investigating the more general problem of the interaction of air pollutants with indoor surfaces.

NOMENCLATURE

C, concentration of species [atoms m^{-3}];

C_o, normalizing constant concentration of species [atoms m^{-3}];

D, diffusivity [$m^2\ s^{-1}$];

g, gravitational acceleration [$m\ s^{-2}$];

Gr, Grashof number, $\frac{g\ \beta\ \Delta T\ H^3}{\nu^2}$;

H, enclosure height [m];

$\hat{k}$, unit vector in the upward direction;

n, coordinate dimension normal to the enclosure surface [m];

P, dimensionless pressure, $\frac{p\ H^2}{\rho\ \nu^2}$;

p, pressure [$kg\ m^{-1}\ s^{-2}$];

Pr, Prandtl number, $\frac{\nu}{\alpha}$;

Ra, Rayleigh number, $Gr \times Pr$;

Sc, Schmidt number, $\frac{\nu}{D}$;

t, time [s];

T, air temperature [K];

ΔT, temperature difference across enclosure, $T_H - T_C$ [K];

T_C, temperature of cool wall [K];

T_H, temperature of hot wall [K];

$\underset{\sim}{U}$, air velocity vector [$m\ s^{-1}$];

$\underset{\sim}{V}$, dimensionless air velocity vector, $\frac{H\ \underset{\sim}{U}}{\nu}$.

Greek symbols

α, fluid thermal diffusivity [$m^2\ s^{-1}$];

β, volumetric coefficient of thermal expansion [K^{-1}];

λ_a, attachment rate of decay products to airborne particles [s^{-1}];

λ_i, radioactive decay constant of species i [s^{-1}];

Λ_i, dimensionless decay constant of species of interest, $\frac{\lambda_i H^2}{\nu}$;

Λ_a, dimensionless attachment rate of decay products to particles, $\frac{\lambda_a H^2}{\nu}$;

ν, kinematic fluid viscosity [$m^2 s^{-1}$];

ρ, fluid density [$kg\ m^{-3}$];

θ, dimensionless temperature, $\frac{2T - T_H - T_C}{T_H - T_C}$;

τ, dimensionless time, $\frac{t\,\nu}{H^2}$;

ω, dimensionless species concentration, $\frac{C}{C_o}$.

Subscripts

212, lead-212;

218, polonium-218;

222, radon-222.

1. INTRODUCTION

The interaction of air pollutants with indoor surfaces is an important phenomenon from two contrasting perspectives. For protecting human health, pollutant reaction with indoor surfaces may be beneficial because it reduces airborne concentrations and corresponding occupant exposures (Sabersky et al., 1973; Weschler et al., 1989). On the other hand, air pollutant deposition may damage surfaces within buildings (Shaver et al., 1983; Sinclair et al., 1988) or interfere with manufacturing processes (Cooper, 1986).

One class of indoor pollutants that has received much attention in the past decade is radon along with its decay products. Inhalation exposure in buildings to the radioactive progeny of ^{222}Rn is responsible for a major portion of the effective radiation dose to the public (Sinnaeve et al., 1984). In the general population, the estimated risk of lung cancer attributable to indoor radon

exposure is much larger than the cancer risk attributable to exposure to most other environmental contaminants (Nero, 1988)* . The concentration of ^{220}Rn is typically smaller than that of ^{222}Rn. Nevertheless, the radiation dose associated with inhalation of ^{220}Rn progeny may also be significant (Schery, 1990).

The radiation exposure of the lung resulting from inhalation of a given level of indoor radon depends on the concentration and size distribution of the short-lived decay products. These factors are significantly influenced by indoor conditions, including the airborne particle concentration, the ventilation rate, and the nature and intensity of indoor air movement. Knutson (1988) and Bruno (1983) have written useful overviews of radon decay product dynamics; a brief summary of the key points is presented below.

As shown in Figure 1, the radioactive decay chains of ^{238}U and ^{232}Th each feature an isotope of radon (^{222}Rn and ^{220}Rn, respectively) followed by a series of short-lived decay products which terminates with a long-lived or stable species (^{210}Pb and ^{208}Pb, respectively). Several characteristics of these decay chains contribute to their radiological health hazard: (a) radon is an inert gas, permitting migration from its site of origin into the atmosphere; (b) several decay products of radon (the shaded isotopes in the figure) have half lives that are long enough to be inhaled and deposited in the respiratory tract, and yet short enough to have a significant probability of decaying before being cleared from the lung; and (c) between each of the shaded isotopes and the termination of the chain is at least one alpha-emitting isotope. Alpha particles deposit their energy over a short range in tissue (~ 50 μm [James, 1988]), and thus can cause significant radiological damage in the vicinity of the site of radioactive decay.

Consider an atom of ^{222}Rn in indoor air. Its decay by alpha-particle emission produces a recoiling ^{218}Po atom. In interacting with air molecules during recoil (the duration of which is of

---

* We note that cigarette smoking and exposure to radon decay products appear to act synergistically as causes of lung cancer. Consequently, much of the total population risk associated with radon exposure is believed to occur in the fraction of the population that smokes (Nazaroff and Teichman, 1990).

the order of a nanosecond), the ^{218}Po loses electrons and so tends to be positively ionized with a single unit of charge effectively at formation. In ordinary indoor environments, ^{218}Po is rapidly neutralized (Hopke, 1988). Both the charged and the neutral species interact with gases, including O_2, H_2O and trace species, to form clusters that have lower diffusivity than the free atom. In any of these forms—charged or neutral, and clustered to various extents—the ^{218}Po species is termed "unattached." The diffusivity of unattached decay products is in the vicinity of 0.05 $cm^2\ s^{-1}$ (Phillips et al., 1988), and is expected to vary with the composition of the surrounding gas.

Among the fates of the unattached decay products is attachment to preexisting airborne particles. The behavior of this "attached" mode is determined by the particle size. The diffusivity of unattached decay products is very much larger than that of the attached species. For example, a spherical particle of diameter 0.1 μm has a diffusivity of $7 \times 10^{-6}\ cm^2\ s^{-1}$ (Hinds, 1982).

Because of their much larger diffusivity, the unattached decay products are believed to pose a much larger hazard, per atom inhaled, than the attached species (James, 1988). In this regard, the most important elements in the decay chains are ^{218}Po for the ^{222}Rn series and ^{212}Pb for the ^{220}Rn series as, among the decay products, the fraction unattached is largest for these species.

Although the health hazard is directly associated with the decay products, assessments of radiological dose from inhalation exposure to radon decay products are commonly based on the more easily measured airborne radon concentration. The research reported here was motivated by the recognition that the rate of deposition of unattached decay products onto indoor surfaces is an important factor governing the relationship between exposure to radon and the radiological exposure of tissues in the respiratory tract.

Studying the deposition of radon decay products onto indoor surfaces can yield additional benefits. Detailed understanding of the mass-transport of radon decay product deposition is needed as a basis for evaluating the effect on human exposure that could result from changes in building design and operation, including the use of filtering devices and other control measures. Also, such investigations might elucidate near-surface air flow conditions in buildings that would, in turn, lead to improved understanding of the rates of reaction of other pollutants with indoor

surfaces (Nazaroff and Cass, 1989). Finally, an experimental technique has been proposed in which long-term average ^{222}Rn concentrations are determined from ^{210}Po alpha activity on glass (Samuelsson, 1988). The relationship between the ^{210}Po alpha activity and the ^{222}Rn concentration is critically dependent on the deposition rate of unattached ^{218}Po.

Studies of the deposition rate of unattached radon decay products onto indoor surfaces have not yet yielded a comprehensive description of the process. Experimental investigations have been conducted in small chambers (George et al., 1983; McLaughlin and O'Byrne, 1984), and in rooms (Scott, 1983; Toohey et al., 1984; Bigu, 1985) but air flow conditions in these experiments have not been adequately reported either to fully interpret the results or to extrapolate to other settings. In recent studies, a homogeneous turbulence particle-deposition model (Crump and Seinfeld, 1981) has been applied in an attempt to explain deposition measurements in chambers (Holub et al., 1988; Vanmarcke, 1991). However, these investigations have not accommodated the fact that the governing equations in the Crump and Seinfeld model do not include terms for radioactive generation and decay. Therefore, this model cannot be directly applied to the analysis and interpretation of radon decay product deposition. Also, while this model predicts uniform deposition velocity for unattached decay products onto all surfaces, experiments have shown that deposition velocity can vary substantially with surface orientation (Scott, 1983).

Our investigations build upon the work of Schiller et al. (1989) and Schiller and Revzan (1989). In those studies, a finite-difference model was employed to investigate the rate of deposition of ^{222}Rn decay products onto surfaces under four air flow regimes: (a) stagnant conditions; (b) forced laminar flow parallel to a flat plate; (c) laminar natural convection flow adjacent to a vertical isothermal flat plate; and (d) two-dimensional laminar natural convection enclosure flow. Among their findings, Schiller et al. reported that the predicted surface-averaged deposition velocity was at the low end of experimental results. The enclosure flow investigated by Schiller et al. was based on boundary conditions that would lead to relatively weak mass transport to horizontal surfaces (i.e., isothermal warm and cool walls connected by an adiabatic top and bottom). Among the issues we sought to address in our investigation was whether boundary

conditions that stimulate stronger near-surface flow would lead to significantly higher deposition velocities. In addition, because Schiller et al. only simulated a single enclosure geometry with two wall-to-wall temperature differences (characterized by Grashof numbers, $Gr = 3 \times 10^9$ and 3×10^{10}), we sought to substantially extend the number of simulations to explore more completely the dependence of deposition on temperature difference, enclosure size, and diffusivity. A third objective of this study was to investigate the deposition of unattached ^{212}Pb. To our knowledge, no previous theoretical work has been reported on the deposition of this species. Because of differences in their rates of generation and decay, ^{212}Pb and ^{218}Po are not expected to deposit at the same rate, even if their diffusivity is the same. This point appears not to have been recognized by other investigators (Bigu, 1985; Knutson, 1988). Finally, because deposition velocity measurements are often based on the deposited activity collected over a small fraction of an enclosure's surface, detailed predictions are presented for the first time of the local deposition velocity.

2. METHODS

Simulations reported in this study entailed the following four steps: (a) specification of an enclosure geometry and suitable boundary conditions; (b) numerical solution of steady-state equations of fluid motion to obtain the air velocity field; (c) numerical solution of the advection-diffusion equation with terms to account for radioactive generation and decay plus attachment to particles, as appropriate, to obtain ^{218}Po or ^{212}Pb concentration fields; and (d) calculation of the local and mean deposition velocity from the species concentration fields.

The simulations correspond to experiments in which a quantity of a radon isotope is initially uniformly dispersed in a chamber in which the thermal boundary conditions are fixed. For the case of ^{222}Rn, the activity concentration of ^{218}Po rapidly rises to a significant fraction of the radon activity concentration, then remains in secular equilibrium. Subsequently, the concentrations of ^{222}Rn and ^{218}Po diminish slowly as governed by the 3.8 d half-life of ^{222}Rn. Experimental measurements of ^{218}Po deposition could be conducted over periods of several minutes, a brief

enough time to approximate the ^{222}Rn concentration as constant. During such experiments, the decay of ^{222}Rn would constitute a constant and spatially uniform source of ^{218}Po. By contrast, if ^{220}Rn were initially dispersed in a chamber, it would decay rapidly and completely through ^{216}Po to ^{212}Pb. The ^{212}Pb concentration would then diminish slowly as governed by its 10.6 h half-life.

During the research reported in this paper, a total of 39 simulations (30 for ^{218}Po and nine for ^{212}Pb) were conducted, investigating three cases of two-dimensional air flow. The first two cases represent idealized conditions of natural convection enclosure flow. The enclosure is square and the two vertical sides are isothermal with one side at a temperature higher than the other by an amount ΔT. In the first case, schematically depicted in Figure 2, the horizontal surfaces are adiabatic. In the second case, the temperatures of the top and bottom surfaces are specified to vary linearly with distance between the warm and cool vertical sides. The third case employs more realistic temperature boundary conditions for natural convection flow in buildings. The surface temperatures for this case were obtained from a study of heat transfer in residential buildings and correspond to predictions for the south-facing zone of a well-insulated, multizone residential structure on a clear, cold winter morning in Albuquerque, NM (Bauman et al., 1983). Infiltration and ventilation are neglected in all cases; i.e., there is assumed to be no air flow across the enclosure boundaries. Incorporating the influence of air flow across boundaries on the enclosure flow field and deposition velocities would not present any intrinsic difficulty in the solution scheme described below.

For each of the three enclosure configurations, predictions of ^{218}Po and ^{212}Pb deposition velocities were generated for baseline conditions in which the rate of attachment to preexisting particles was taken to be zero. The baseline conditions for Cases 1 and 2 specified the enclosure dimensions to be 3 m $\times$ 3 m and the temperature difference between the vertical sides to be 4 K. Details of Case 3 baseline conditions are presented in Figure 3. For each case, we explored the effect of attachment to particles on the predicted deposition velocity. In addition, for Case 1, we explored the effect on the ^{218}Po deposition velocity of varying three key parameters: the ^{218}Po

diffusion coefficient (D), the wall-to-wall temperature difference (ΔT), and the enclosure size (H). The parameter ranges over which simulations were executed are presented in Table 1.

For each simulation, the air velocity fields were obtained by means of a finite difference numerical model. The model employed the Patankar-Spalding differencing scheme to solve the steady-state equations of fluid motion (1-3) with the Boussinesq approximation (Gadgil, 1980):

Continuity:[a]
$$\underset{\sim}{\nabla}^* \cdot \underset{\sim}{V} = 0 \qquad (1)$$

Momentum:
$$(\underset{\sim}{V} \cdot \underset{\sim}{\nabla}^*)\, \underset{\sim}{V} = \nabla^{*2} \underset{\sim}{V} - \underset{\sim}{\nabla}^* P + Gr\, \theta\, \hat{k} \qquad (2)$$

Energy:
$$\underset{\sim}{V} \cdot \underset{\sim}{\nabla}^* \theta = \frac{1}{Pr} \nabla^{*2} \theta \qquad (3)$$

where $\underset{\sim}{V}$, P, and θ represent dimensionless air velocity, pressure, and temperature, respectively, and $\hat{k}$ is the unit vector in the direction opposite gravity. The boundary conditions for these simulations stipulated that there was no slip at the enclosure surfaces and that each segment of the surfaces either had a specified temperature or was adiabatic. The effect of temperature on the viscosity and thermal diffusivity of air was ignored. A Prandtl number (Pr) of 0.71, corresponding to T=293 K, was used in the simulations.

In the solution procedure, the enclosure area was divided into subregions, each represented by a grid node. Grid spacing in the computational domain was varied in geometric progression with much higher spatial resolution near surfaces. Employing a variable grid size permitted accurate predictions of concentration profiles in near-surface regions while limiting computational costs. The solutions were tested for robustness with respect to changes in grid density and convergence criteria.

---

[a] $\nabla^* = \nabla H$

The solution algorithm employed iterative under-relaxation of the time-dependent versions of equations (1-3) to approach solution of the steady-state equations. Iterations were terminated when successive fractional changes (i.e., residues) in the pressure field at all nodes became smaller than 10^{-6}. A typical solution for the air velocity field using a 29×29 grid required 9 minutes of CPU time on a Cray X-MP.

The nature of near-surface natural convection flow is a function of the Grashof number or the Rayleigh number ($Ra = Gr \times Pr$). For flow along a vertical surface, the Rayleigh number may be physically interpreted as the fourth power of the ratio of surface height to boundary-layer thickness (Bejan, 1984). For room-sized enclosures, a value of $Ra \sim O(10^9)$ is common. The corresponding fluid-mechanical boundary-layer thickness along the walls is O(1 cm).

Fluid velocity, temperature and heat transfer predictions obtained from the natural-convection enclosure model have been satisfactorily compared with experimental and analytical results for laminar enclosure flows at Rayleigh numbers appropriate for room-sized enclosures (Shiralkar et al., 1981; Tichy and Gadgil, 1982; Gadgil and Gobin, 1984; Gadgil et al., 1984). Experimental evidence (Nansteel and Grief, 1981; Bauman et al., 1983) indicates that the transition to turbulence in an enclosure is delayed beyond the transition Ra value observed for free-wall boundary layers to about 10^{10}. For the simulations in this paper, the upper end of the range of Ra values probably extends into the transition regime; however, laminar flow conditions are presumed to prevail.

Once the velocity field was determined for specified geometry and thermal boundary conditions, a similar finite-difference model was employed to obtain the concentration field for ^{218}Po or ^{212}Pb. The numerical approach described above was employed to solve a species conservation equation (4 or 5):

Conservation of ^{218}Po:

$$\underset{\sim}{V} \cdot \underset{\sim}{\nabla}^* \omega_{218} = \frac{1}{Sc_{218}} \nabla^{*2} \omega_{218} + \Lambda_{222}\, \omega_{222} - \Lambda_{218}\, \omega_{218} - \Lambda_a\, \omega_{218} \qquad (4)$$

Conservation of ^{212}Pb:

$$\frac{\partial \omega_{212}}{\partial \tau} + \underset{\sim}{V} \cdot \underset{\sim}{\nabla^*} \omega_{212} = \frac{1}{Sc_{212}} \nabla^{*2} \omega_{212} - \Lambda_{212}\, \omega_{212} - \Lambda_a\, \omega_{212} \qquad (5)$$

The terms in equation (4) account, respectively, for advection, diffusion, radioactive generation, radioactive decay, and attachment to particles, respectively. In accordance with the qualitative differences in the decay chains of ^{222}Rn and ^{220}Rn, the two decay products are treated differently in these equations. For ^{218}Po, a steady-state solution is sought in which its rate of generation ($\Lambda_{222}\, \omega_{222}$) is constant, corresponding to a concentration of ^{222}Rn that is presumed to be constant throughout the enclosure. For ^{212}Pb, a transient "pseudo-steady state" solution is sought in which there is no generation by precursor decay.

Base-case diffusion coefficients were taken as the mean of experimental observations reviewed by Phillips et al. (1988): 0.056 $cm^2\ s^{-1}$ for ^{218}Po and 0.047 $cm^2\ s^{-1}$ for ^{212}Pb. Reported diffusivity values span a large range, so simulations were conducted for ^{218}Po diffusivities varying from 0.02 to 0.1 $cm^2\ s^{-1}$.

The boundary conditions for equations (4) and (5) correspond to perfectly absorbing walls:

$$\omega_{218} = 0 \text{ at all surfaces} \qquad (6)$$

$$\omega_{212} = 0 \text{ at all surfaces} \qquad (7)$$

For the time-dependent ^{212}Pb simulations, the initial condition was

$$\omega_{212} = 1 \text{ at all positions in the enclosure} \qquad (8)$$

The rate of deposition of air pollutants to surfaces is conventionally reported in terms of the deposition velocity, a mass-transfer coefficient that represents the contaminant flux density to a surface divided by the concentration far from the surface. This convention is followed here, with

the flux computed as the product of the diffusion coefficient and the normal component of the concentration gradient at the wall. The deposition velocity is then evaluated as

$$v_d = - \frac{D}{\omega_i(\text{core})} \left(\frac{\partial \omega_i}{\partial n} \right)_{n=0} \qquad (9)$$

where n represents the coordinate dimension normal to the surface. The concentration gradient term in equation (9) was calculated from the grid line closest to each surface. The accuracy of the calculation was checked by (a) confirming that the normal component of the concentration gradient did not change through the second grid line from each surface and (b) that the advective flux normal to the surface at the first grid line was negligible compared with the diffusive flux. To achieve a high degree of accuracy, the first grid lines were placed approximately 0.1 cm from the surfaces.

The normalizing species concentration, ω_i(core), was taken to be the spatially weighted average of the central 85% of the chamber's area. Because of uniform generation throughout the space, the core concentration of ^{218}Po was relatively uniform: the average core concentration for the central 2% of the the chamber area only differed from the average for the central 85% by 4-8% for the basic conditions in Cases 1 through 3. On the other hand, the concentration varied substantially through the core region for ^{212}Pb. For basic conditions in Cases 1 through 3, the central 2% of the chamber area had an average ^{212}Pb concentration that was 18-56% higher than that for the central 85% of the chamber area. Consequently, the deposition velocity results for ^{212}Pb are sensitive to the specific definition of the core region.

For most of the simulations reported here, the rate of attachment of radon decay products to airborne particles was taken to be zero. However, for baseline conditions in each of the three cases, we have conducted simulations with attachment rates of 5 h^{-1} and 50 h^{-1}, corresponding to low and typical airborne particle concentrations in rooms (Knutson, 1988). The attachment rate was assumed to be constant throughout the enclosure.

4. RESULTS AND DISCUSSION

Important results from the numerical simulations are presented in Figures 4-10 and in Tables 2 and 3. Figures 4-7 emphasize the dependence of deposition rate on position and demonstrate differences between ^{218}Po and ^{212}Pb. Figures 8-10 address the effect of potentially significant variables—diffusivity (D), vertical-side temperature difference (ΔT) and enclosure dimension (H)—on the overall average deposition velocity of ^{218}Po for the Case 1 enclosure conditions in the absence of attachment to particles.

One particularly striking result is the strong dependence of deposition velocity on position along the enclosure surface. Figures 4-7 each show more than an order of magnitude difference between the maximum and minimum values of the deposition velocities for both species. The largest deposition velocities occur near the corners. This result was surprising, since we expected a thicker boundary layer and consequently a lower deposition velocity near the corners. Examination of the velocity fields revealed the explanation: the rapid change in flow direction near the corners is associated with significant near-surface velocities toward the surfaces. This phenomenon is illustrated for Case 1 in Figure 6. In the lower corner of the warm wall (lower left frame of the figure), the rapid acceleration of flow along the vertical surface is seen to induce a downward velocity component outside of the boundary layer. Advective transport towards the surface enhances the deposition velocity to a local peak value at a normalized distance of 3.995 from the reference corner, as seen in the lower right frame of Figure 6. Likewise, a horizontal velocity component towards the wall is observed above the lower left corner, again leading to enhanced local deposition. In the upper corner of the warm wall, an eddy is induced by the rapid deceleration and change in flow direction. The diagram in the upper left frame of Figure 6 shows substantial flow towards the surface near the upper corner of the warm wall.

In addition, at each corner of the enclosure, a local minimum in deposition velocity is observed. This minimum results from a combination of low air velocity in the corner and depleted

species concentration owing to upstream deposition. The patterns displayed in Figure 6 are qualitatively reproduced in the other simulations.

A comparison of Figures 3 and 7 reveals that the deposition velocity is also large wherever natural convection is strong. The central surface segment shown along the left side in Figure 3 (temperature of 6.1 °C) represents a window. Because of the large temperature difference between the surface and the air, the air velocity adjacent to this surface is large and the species concentration boundary layer is correspondingly thin. Consequently, the local deposition velocity is much larger than the value elsewhere other than near the corners.

A second important result of these simulations is the qualitative difference in behavior of ^{218}Po and ^{212}Pb. Figure 4 illustrates this point. The maximum deposition velocity for ^{218}Po occurs near the reference corner (normalized distance ~ 0), upstream of the flow along the vertical side, whereas the maximum deposition velocity for ^{212}Pb occurs in the corner downstream of the flow along the vertical side (normalized distance ~ 1). Furthermore, as shown in Table 2, the deposition velocity in Case 1 for ^{218}Po averages 2.7 times the corresponding value for ^{212}Pb. By contrast, in Case 3, the difference between average ^{218}Po and ^{212}Pb deposition velocities is only 15%, roughly consistent with the assumed difference in diffusivity between the species.

The explanation for these observations centers on the differences the radioactive decay chains for these species. The key distinction becomes evident when comparing half-lives for radioactive decay of the species with the characteristic time for air within a boundary layer to travel the length of an enclosure surface. For the simulations considered here, characteristic times for air flow along surfaces are of the order of a minute, comparable to the ^{218}Po half-life (3.04 min) and negligible compared with the ^{212}Pb half-life (10.6 h). Consequently, radioactive production and decay within the boundary layers adjacent to surfaces are important for ^{218}Po, whereas ^{212}Pb behaves much as would a nonradioactive species.

Figures 8 and 9 show that the effects of diffusion coefficient and enclosure-side temperature difference on deposition velocity are substantial. A larger diffusivity implies more rapid transport to surfaces. An increased temperature difference decreases the size of the boundary

layer, yielding higher deposition velocities, most significantly on vertical surfaces. With all else held constant, the effect of enclosure size (Figure 10) is small.

Our results are consistent with earlier and more limited findings of Schiller and Revzan (1989). The enclosure conditions they simulated are the same as our Case 1. For a 3 m × 3 m enclosure, with $\Delta T = 0.85$ K, $\lambda_a = 0$, and $D = 0.054$ cm^2 s^{-1}, they found an average deposition velocity for unattached ^{218}Po of 0.20 mm s^{-1}. Figure 9 shows that for the same conditions except for a slightly higher value of D (0.056 cm^2 s^{-1}), we obtained an average deposition velocity of 0.23 mm s^{-1}.

The effect of attachment to particles on deposition velocity of the unattached species is moderate, as shown in Table 3. Qualitatively, the effect of attachment is analogous to the effect of radioactive decay. By providing an alternative fate to deposition, these removal processes alter concentration profiles in the boundary layers. Attachment reduces the deposition flux density, but the core concentration is reduced to an even greater extent, so that the deposition velocity increases with increasing attachment. The generation of ^{218}Po by ^{222}Rn decay causes the influence of attachment on deposition velocity to be smaller for ^{218}Po than for ^{212}Pb.

5. CONCLUDING REMARKS

We have simulated the deposition of unattached radon decay products—^{218}Po and ^{212}Pb—onto the surfaces of two-dimensional enclosures in which air flow is laminar and driven by natural convection. The deposition velocity is found to be a sensitive function of position, particularly near corners. Along flat surfaces, the higher values correspond with conditions that would lead to higher heat transfer rates.

Under flow conditions in which the core air does not mix rapidly with the boundary layer (Cases 1 and 2), the deposition velocity is much larger for ^{218}Po than for ^{212}Pb. The explanation for this observation lies in the details of the radioactive decay chains: ^{218}Po deposition is enhanced because it is continually produced by the decay of ^{222}Rn whose concentration is constant throughout the space. The average distance through which ^{218}Po atoms must migrate to deposit is

reduced by this mechanism compared with ^{212}Pb which must be transported from the core through the full boundary layer.

The deposition velocity increases with increasing species diffusivity. It also increases as air velocities increase, as shown by the relationship between mean deposition velocity and temperature difference across vertical enclosure sides. Attachment to particles leads to moderate increases in the deposition velocity. The effect of enclosure size is found to be small.

Boundary conditions that increase the intensity of near-surface flows increase the average deposition velocity. Table 2 shows that over the range of conditions considered in this work, the effect is relatively small for ^{218}Po—60% difference between Cases 2 and 3. The impact is much larger for ^{212}Pb—the average deposition velocity is 3.5 times higher for Case 3 than for Case 2. Furthermore, large variations in local deposition velocity indicate that the positional dependence of the deposition velocity is strongly influenced by the air flow field.

For the three cases considered, even including the effects of attachment, the average deposition velocity for ^{218}Po, 0.23-0.49 mm/s, is much smaller than the value 2.2 mm/s (8 m/h) suggested by Knutson (1988) on the basis of experiments to be a "representative average" over the surfaces of a typical room. The predicted peak local values are closer to these experimental results.

It is important to investigate further the discrepancy between experimental observations and theoretical predictions of unattached ^{218}Po deposition velocity. The research community cannot be completely confident in its understanding of unattached decay product deposition until experimental and theoretical results are reconciled. Experiments to measure the unattached decay product deposition velocity must be designed and conducted under conditions in which air flow near surfaces is well characterized. Comparing theory with experiment in such a setting is an essential step toward resolving the differences yielded by the two approaches. Efforts to improve our understanding of air motion in rooms are also needed.

Acknowledgements—This research was supported by the Universitywide Energy Research Group of the University of California, and by the Director, Office of Energy Research, Office of Health

and Environmental Research, Human Health and Assessments Division and Pollutant Characterization and Safety Research Division of the U. S. Department of Energy under Contract No. DE-AC03-76SF00098. Additional support was provided by a grant from the Berkeley Engineering Fund. We thank D. Gobin for assistance with reinstalling the numerical fluid mechanics software at Lawrence Berkeley Laboratory during the early stages of this work. F. Bauman, K. Revzan, and R. Sextro provided useful review comments on the draft manuscript.

References

Bauman, F., Gadgil, A., Kammerud, R., Altmayer, E. and Nansteel, M. (1983) Convective heat transfer in buildings: Recent research results, *ASHRAE Trans.*, **89(1A)**, 215.

Bejan, A. (1984) *Convection Heat Transfer*, Wiley, New York.

Bigu, J. (1985) Radon daughter and thoron daughter deposition velocity and unattached fraction under laboratory-controlled conditions and in underground uranium mines, *J. Aerosol Sci.*, **16**, 157.

Bruno, R. C. (1983) Verifying a model of radon decay product behavior indoors, *Health Phys.*, **45**, 471.

Cooper, D. W. (1986) Particulate contamination and microelectronics manufacturing: An introduction, *Aerosol Sci. Technol.*, **5**, 287.

Crump, J. G. and Seinfeld, J. H. (1981) Turbulent deposition and gravitational sedimentation of an aerosol in a vessel of arbitrary shape, *J. Aerosol Sci.*, **12**, 405.

Gadgil, A. J. (1980) On convective heat transfer in building energy analysis, Ph. D. thesis, Physics Department, University of California, Berkeley.

Gadgil, A. J. and Gobin, D. (1984) Analysis of two-dimensional melting in rectangular enclosure in the presence of convection, *J. Heat Transfer, Trans. ASME*, **106**, 20.

Gadgil, A. J., Bauman, F., Altmayer, E. and Kammerud, R. (1984) Verification of a numerical simulation technique for natural convection, *J. Solar Energy Eng., Trans. ASME*, **106**, 366.

George, A. C., Knutson, E. O. and Tu, K. W. (1983) Radon daughter plateout—I: Measurements, *Health Phys.*, **45**, 439.

Hinds, W. C. (1982) *Aerosol Technology: Properties, Behavior, and Measurement of Airborne Particles*, Wiley, New York, p. 407.

Holub, R. F., Raes, F., Van Dingenen, R. and Vanmarcke, H. (1988) Deposition of aerosols and unattached radon daughters in different chambers; Theory and experiment, *Radiat. Prot. Dosim.*, **24**, 217.

Hopke, P. K. (1988) The initial atmospheric behavior of radon decay products, report DOE/ER-0375, U. S. Department of Energy, Office of Health and Environmental Research, Washington, DC.

James, A. C. (1988) Lung dosimetry, in *Radon and Its Decay Products in Indoor Air* (Edited by Nazaroff, W. W. and Nero, A. V.) p. 259, Wiley, New York.

Knutson, E. O. (1988) Modeling indoor concentrations of radon's decay products, in *Radon and Its Decay Products in Indoor Air* (Edited by Nazaroff, W. W. and Nero, A. V.) p. 161, Wiley, New York.

McLaughlin, J. P. and O'Byrne, F. D. (1984) The role of daughter product plateout in passive radon detection, *Radiat. Prot. Dosim.*, **7**, 115.

Nansteel, M. W. and Grief, R. (1981) Natural convection heat transfer in undivided and partially divided rectangular enclosures, *J. Heat Transfer, Trans. ASME*, **103**, 623.

Nazaroff, W. W. and Cass, G. R. (1989) Mass-transport aspects of pollutant removal at indoor surfaces, *Environ. Int.*, **15**, 567.

Nazaroff, W. W. and Teichman, K. Y. (1990) Indoor radon: Exploring U. S. federal policy for controlling human exposures, *Environ. Sci. Technol.*, **24**, 774.

Nero, A. V. (1988) Controlling indoor air pollution, *Scientific American*, **285(5)**, 42.

Phillips, C. R., Khan, A. and Leung, H. M. Y. (1988) The nature and determination of the unattached fraction of radon and thoron progeny, in *Radon and Its Decay Products in Indoor Air* (Edited by Nazaroff, W. W. and Nero, A. V.) p. 203, Wiley, New York.

Sabersky, R. H., Sinema, D. A. and Shair, F. H. (1973) Concentrations, decay rates, and removal of ozone and their relation to establishing clean indoor air, *Environ. Sci. Technol.*, **7**, 347.

Samuelsson, C. (1988) Retrospective determination of radon in houses, *Nature*, **334**, 338.

Schery, S. D. (1990) Thoron in the environment, *J. Air Waste Manage. Assoc.*, **40**, 493.

Schiller, G. E., and Revzan, K. L. (1989) Transport and deposition of indoor radon decay products: Part 2—Influence of environmental conditions, report LBL-28023, Lawrence Berkeley Laboratory, Berkeley, CA; submitted to *Atmos. Environ.*

Schiller, G. E., Nero, A. V. and Tien, C. L. (1989) Transport and deposition of indoor radon decay products: Part 1—Model development and validation, report LBL-28022, Lawrence Berkeley Laboratory, Berkeley, CA; submitted to *Atmos. Environ.*

Scott, A. G. (1983) Radon daughter deposition velocities estimated from field measurements, *Health Phys.*, **45**, 481.

Shaver, C. L., Cass, G. R. and Druzik, J. R. (1983) Ozone and the deterioration of works of art, *Environ. Sci. Technol.*, **17**, 748.

Shiralkar, G., Gadgil, A. J., and Tien, C. L. (1981) High Rayleigh number convection in shallow enclosures with different end temperatures, *Int. J. Heat Mass Transfer*, **24**, 10.

Sinclair, J. D., Psota-Kelty, L. A. and Weschler, C. J. (1988) Indoor/outdoor ratios and indoor surface accumulations of ionic substances at Newark, New Jersey, *Atmos. Environ.*, **22**, 461.

Sinnaeve, J., Clemente, G. and O'Riordan, M. (1984) The emergence of natural radiation, *Radiat. Prot. Dosim.*, **7**, 15.

Tichy, J. and Gadgil, A. J. (1982) High Rayleigh number laminar convection in low aspect ratio enclosures with adiabatic horizontal walls and differentially heated vertical walls, *J. Heat Transfer, Trans. ASME*, **104**, 103.

Toohey, R. E., Essling, M. A., Rundo, J. and Hengde, W. (1984) Measurements of the deposition rates of radon daughters on indoor surfaces, *Radiat. Prot. Dosim.*, **7**, 143.

Vanmarcke, H., Landsheere, C., Van Dingenen, R., and Poffijn, A. (1991) Influence of turbulence on the deposition rate constant of the unattached radon decay products, *Aerosol Sci. Technol.*, **14**, 257.

Weschler, C. J., Shields, H. C. and Naik, D. V. (1989) Indoor ozone exposures, *JAPCA*, **39**, 1562.

TABLE 1. Range of parameter values considered in Case 1 simulations

symbol	range of values	parameter
H	0.5 - 4.07 m	size of enclosure
ΔT	0.4 - 20 K	temperature difference between vertical sides
D	0.025 - 0.1 $cm^2\ s^{-1}$	diffusion coefficient of ^{218}Po
Gr	7×10^7 - 8×10^{10}	Grashof number
λ_a	0 - 50 h^{-1}	rate of attachment to airborne particles

TABLE 2. Summary of deposition velocities (mm/s) for baseline simulation conditions [a]

Case	^{218}Po	^{212}Pb
Case 1 - Baseline conditions [b]		
Overall average	0.30	0.12
Vertical sides—average	0.43	0.19
Horizontal sides—average	0.17	0.06
Minimum	0.06	0.02
Maximum	0.83	0.45
Case 2 - Baseline conditions [c]		
Overall average	0.23	0.09
Vertical sides—average	0.29	0.12
Horizontal sides—average	0.16	0.07
Minimum	0.02	0.005
Maximum	0.86	0.50
Case 3 [d]		
Overall average	0.37	0.32
Vertical sides—average	0.51	0.45
Horizontal sides—average	0.28	0.23
Minimum	0.03	0.02
Maximum	2.9	2.8

[a] Diffusivities, D: ^{218}Po—0.056 $cm^2\ s^{-1}$; ^{212}Pb—0.047 $cm^2\ s^{-1}$; attachment rate, $\lambda_a = 0$.

[b] Square enclosure, isothermal vertical sides, adiabatic top and bottom; dimension H = 3 m; side-to-side temperature difference $\Delta T = 4$ K (see Figure 2).

[c] Square enclosure, isothermal vertical sides, linear temperature profile along top and bottom; dimension H = 3 m; side-to-side temperature difference $\Delta T = 4$ K.

[d] Rectangular enclosure; dimensions and temperature specification along perimeter as shown in Figure 3.

TABLE 3. Effect of attachment to particles on deposition velocities [a]

Case	^{218}Po			^{212}Pb		
attachment rate, λ_a (h^{-1}) →	0	5	50	0	5	50
Case 1 - Baseline conditions [b]						
Overall average	0.30	0.33	0.44	0.12	0.31	0.81
Vertical sides—avg.	0.43	0.45	0.53	0.19	0.47	1.32
Horizontal sides—avg.	0.17	0.20	0.34	0.06	0.13	0.30
Case 2 - Baseline conditions [c]						
Overall average	0.23	0.25	0.40	0.09	0.41	1.7
Vertical sides—avg.	0.29	0.32	0.47	0.12	0.56	2.3
Horizontal sides—avg.	0.16	0.18	0.33	0.07	0.26	1.1
Case 3 [d]						
Overall average	0.37	0.39	0.49	0.32	0.40	0.63
Vertical sides—avg.	0.51	0.53	0.63	0.45	0.57	0.94
Horizontal sides—avg.	0.28	0.29	0.39	0.23	0.28	0.43

[a] Diffusivities, D: ^{218}Po—0.056 $cm^2\ s^{-1}$; ^{212}Pb—0.047 $cm^2\ s^{-1}$; deposition velocities given in mm/s units.

[b] Square enclosure, isothermal vertical sides, adiabatic top and bottom; dimension H = 3 m; side-to-side temperature difference ΔT = 4 K (see Figure 2).

[c] Square enclosure, isothermal vertical sides, linear temperature profile along top and bottom; dimension H = 3 m; side-to-side temperature difference ΔT = 4 K.

[d] Rectangular enclosure; dimensions and temperature specification along perimeter as shown in Figure 3.

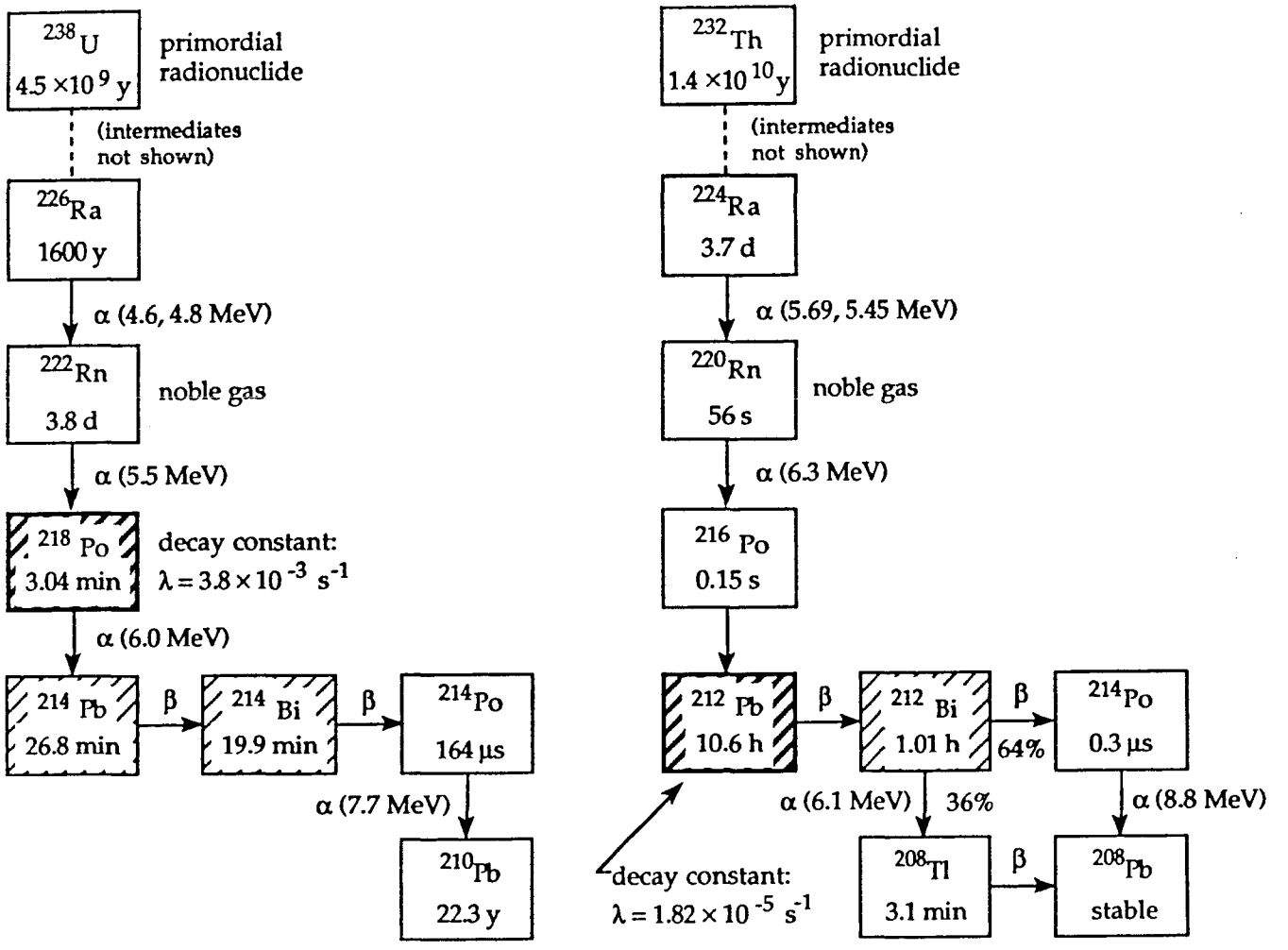

FIGURE 1. Decay chains of uranium-238 to lead-210 and thorium-232 to lead-208, showing the half-life of each isotope, and its mode of decay. Inhalation of the shaded isotopes is the primary health concern. If inhaled and retained in the respiratory tract, the decay from the shaded isotopes to the long-lived or stable lead isotope produces one or two alpha particles that cause damage to tissue adjacent to the decay site. The deposition of unattached ^{218}Po and ^{212}Pb, respectively, onto indoor surfaces is an important factor governing the relationship between the concentration of ^{222}Rn and ^{220}Rn, respectively, and radiation exposure to the lung.

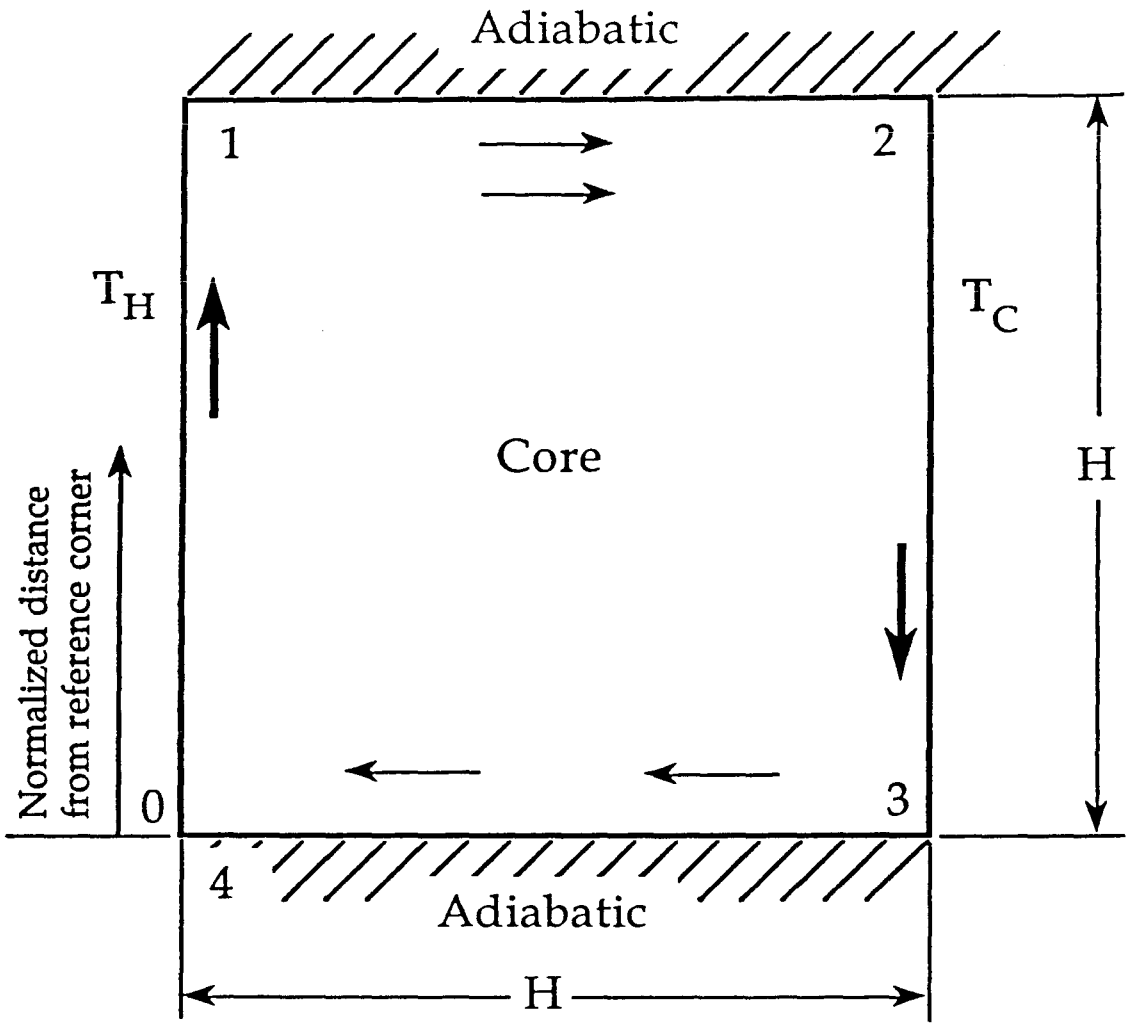

FIGURE 2. Schematic diagram of the enclosure geometry and thermal boundary conditions for simulations in Case 1. The enclosure is square and aligned with the gravitational force; the differentially heated vertical sides are isothermal, and the horizontal sides are adiabatic. The numbers near the corners correspond to positions along the horizontal axis in Figure 4. The Grashof number for the base case flow is 1.6×10^{10}, for an enclosure size 3 m × 3 m and a wall-to-wall temperature difference of 4 K.

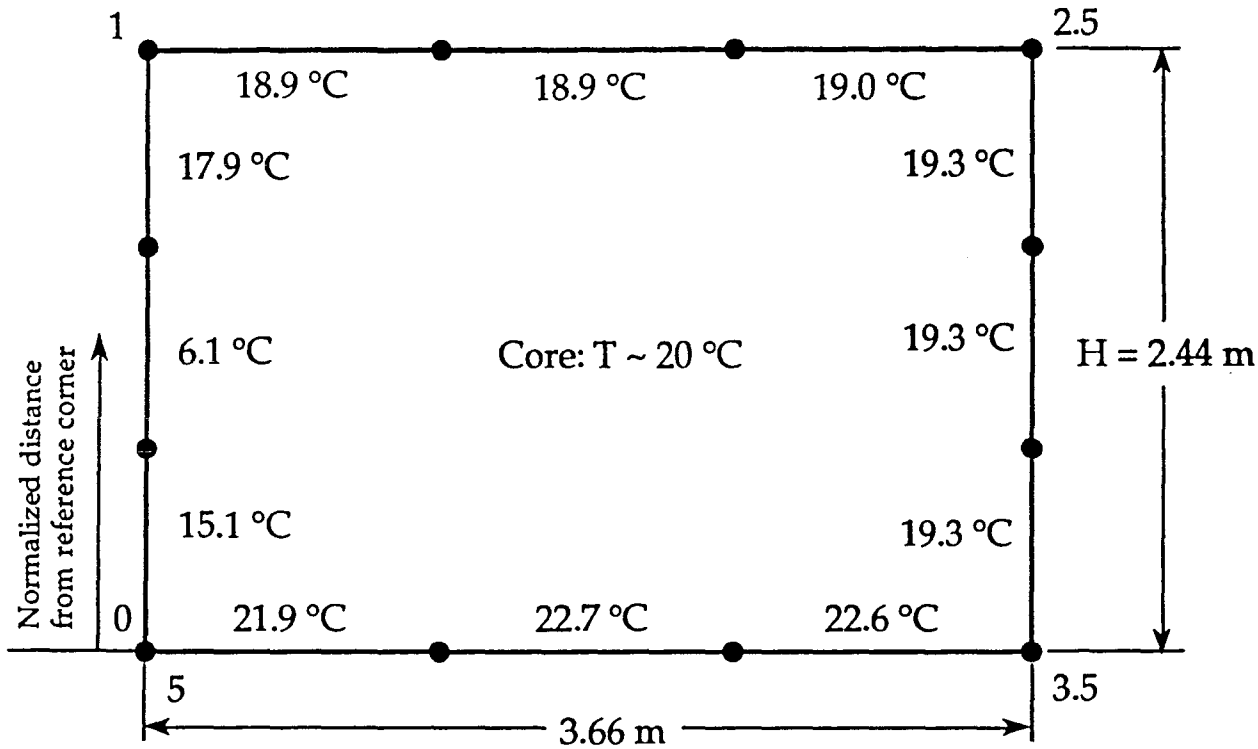

FIGURE 3. Schematic diagram of the enclosure geometry and thermal boundary conditions simulated in Case 3 and corresponding to a room in a residential building (Bauman, 1983). Between each pair of consecutive dots, the temperature of the surface was taken to be constant at the specified value. The numbers labelling the corners correspond to positions along the horizontal axis in Figure 7.

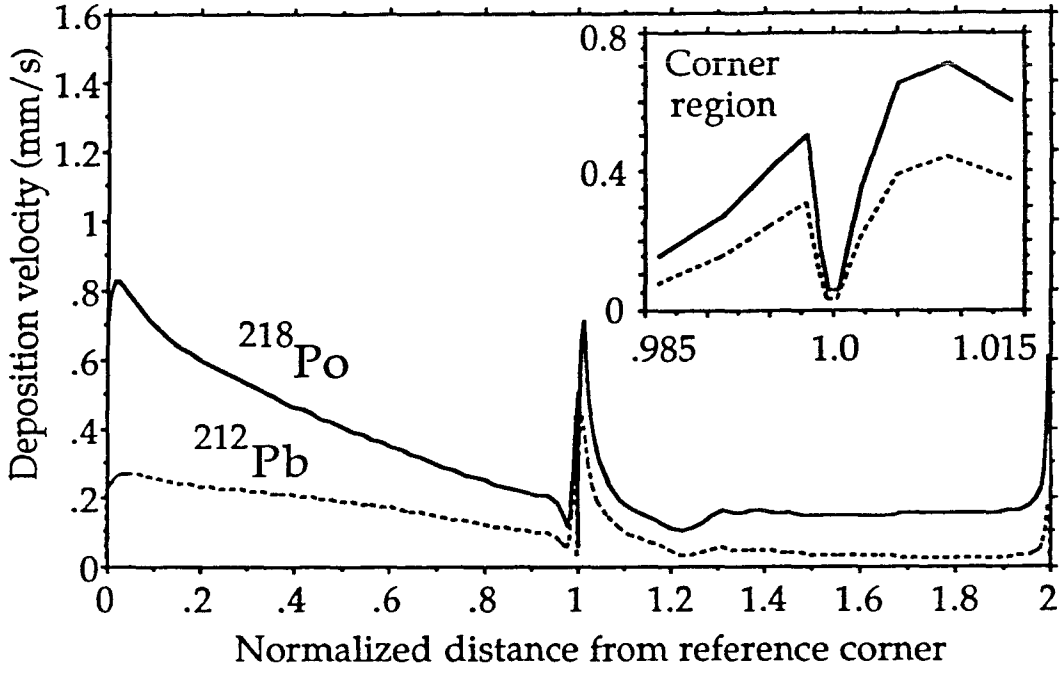

FIGURE 4. Deposition velocity as a function of position for base-case conditions in Case 1 (square enclosure; differentially heated vertical sides; adiabatic top and bottom; see Figure 2). The diffusion coefficients, D, are 0.056 $cm^2\ s^{-1}$ for ^{218}Po and 0.047 $cm^2\ s^{-1}$ for ^{212}Pb. The attachment rate is $\lambda_a = 0$, the enclosure dimension is H = 3 m and the temperature difference between the sides is $\Delta T = 4$ K. The problem was analyzed using a 61 × 61 grid. The deposition pattern presented for normalized distances from 0 to 2 is repeated for normalized distances from 2 to 4. The inset provides details of deposition velocity versus position in the downstream corner of the vertical surface.

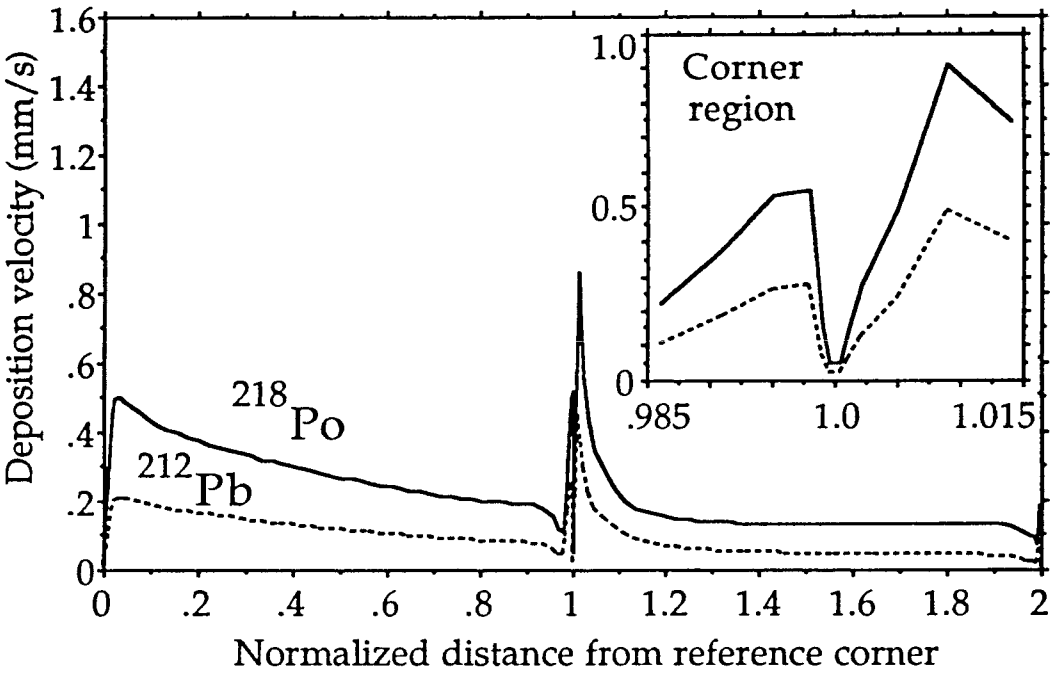

FIGURE 5. Deposition velocity as a function of position for Case 2 (square enclosure; differentially heated vertical sides; linear temperature profile along top and bottom). The diffusion coefficients, D, are 0.056 $cm^2\ s^{-1}$ for ^{218}Po and 0.047 $cm^2\ s^{-1}$ for ^{212}Pb. The attachment rate is $\lambda_a = 0$, the enclosure dimension is H = 3 m and the temperature difference between the sides is $\Delta T = 4$ K. The problem was analyzed using a 61×61 grid. The deposition pattern presented for normalized distances from 0 to 2 is repeated for normalized distances from 2 to 4. The inset provides details of deposition velocity versus position in the downstream corner of the vertical surface.

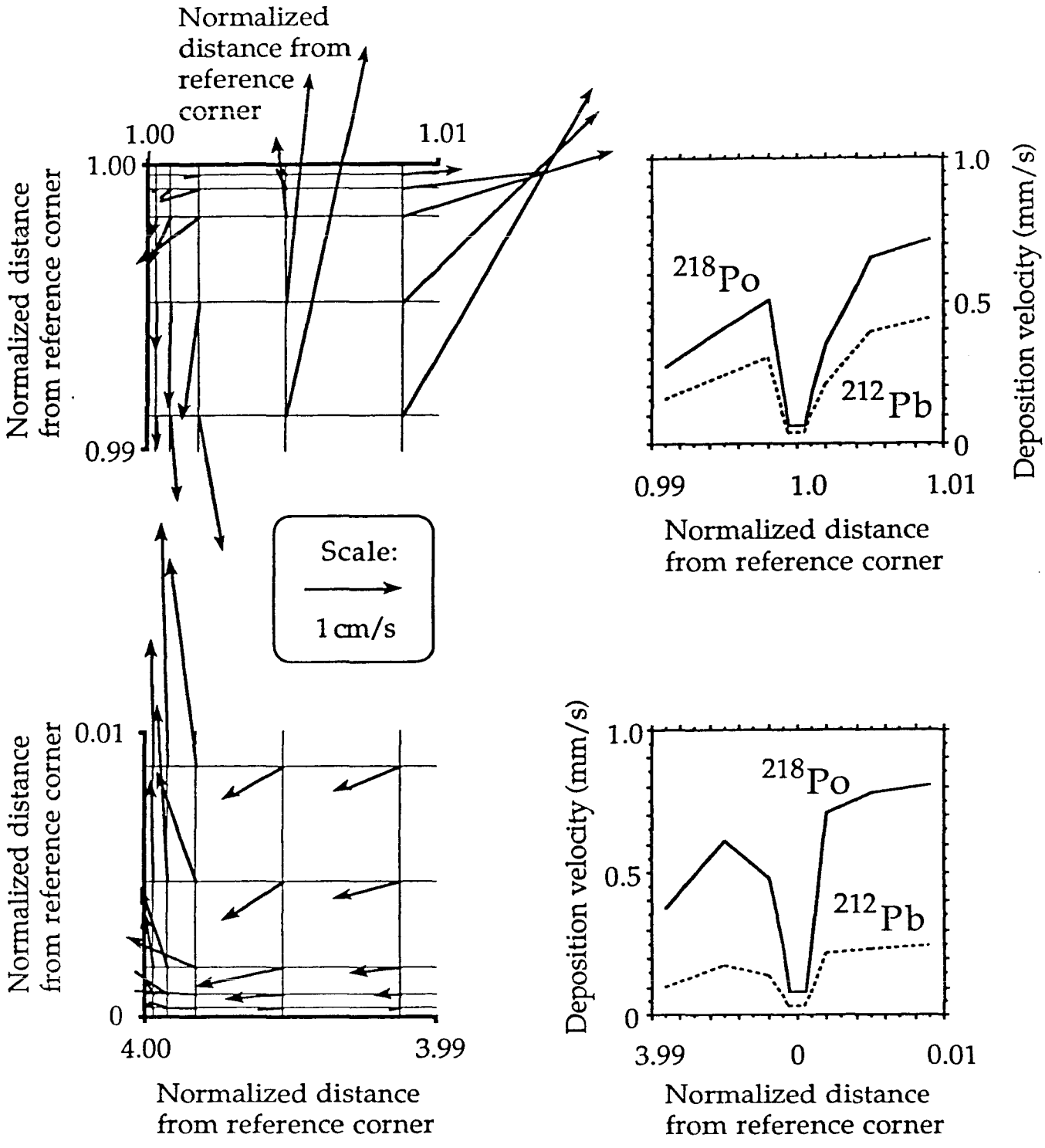

FIGURE 6. Details of air flow and species deposition velocity near left-hand corners for Case 1 (see Figure 2). The regions being explored have an area of 3 cm × 3 cm. The frames on the left show velocity vectors, interpolated from numerical predictions for staggered grids. Arrows are omitted from some lines for clarity. The frames on the right show deposition velocity as a function of position near the respective upper and lower corners of the enclosure.

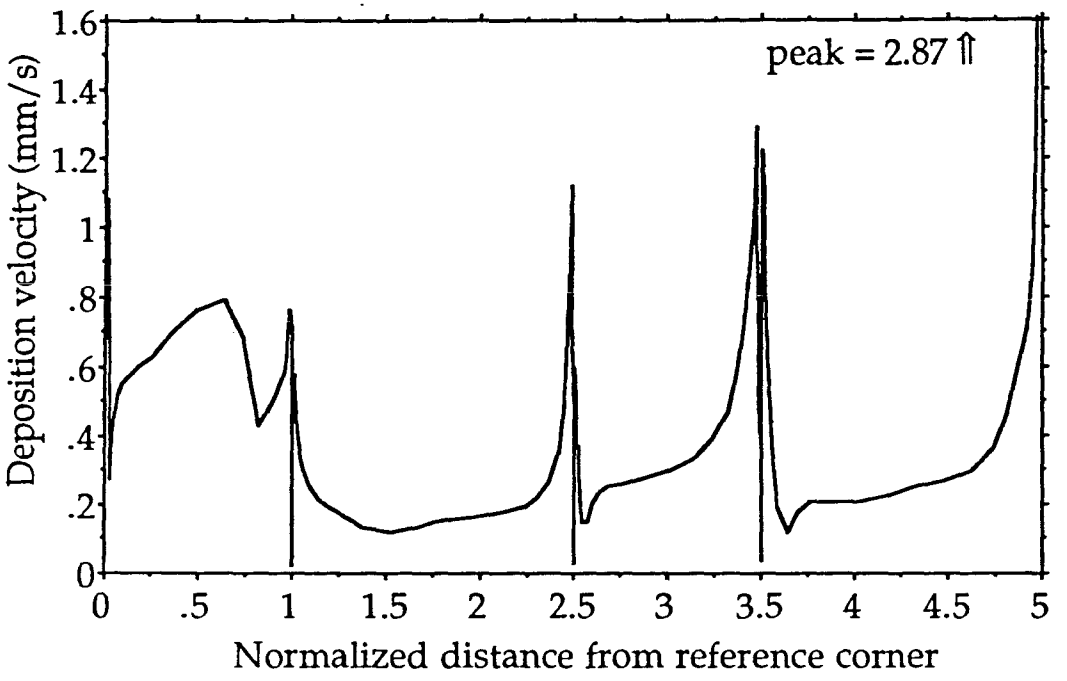

FIGURE 7. Deposition velocity for ^{218}Po as a function of position for Case 3 (rectangular enclosure with temperature specified along full perimeter; see Figure 3). The diffusion coefficient, D, is 0.056 $cm^2\ s^{-1}$. The attachment rate is $\lambda_a = 0$. The problem was analyzed using a 35 (high) × 37 (wide) grid. For clarity, the deposition velocity of ^{212}Pb is not shown; however, the results are similar (see summary in Table 2.

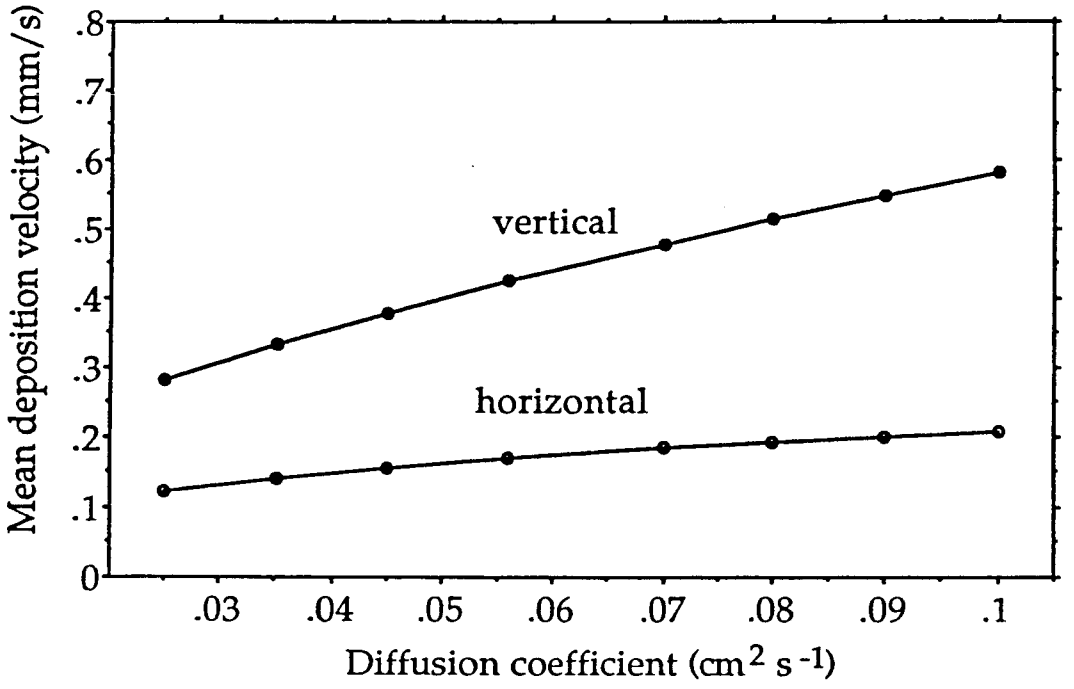

FIGURE 8. Mean deposition velocity of ^{218}Po over enclosure sides as a function of diffusion coefficient, D, for Case 1 geometry (see Figure 2). The attachment rate is $\lambda_a = 0$, the temperature difference between the vertical sides is fixed at $\Delta T = 4$ K, and the enclosure dimension is H = 3 m. The problem was analyzed using a 29×29 grid.

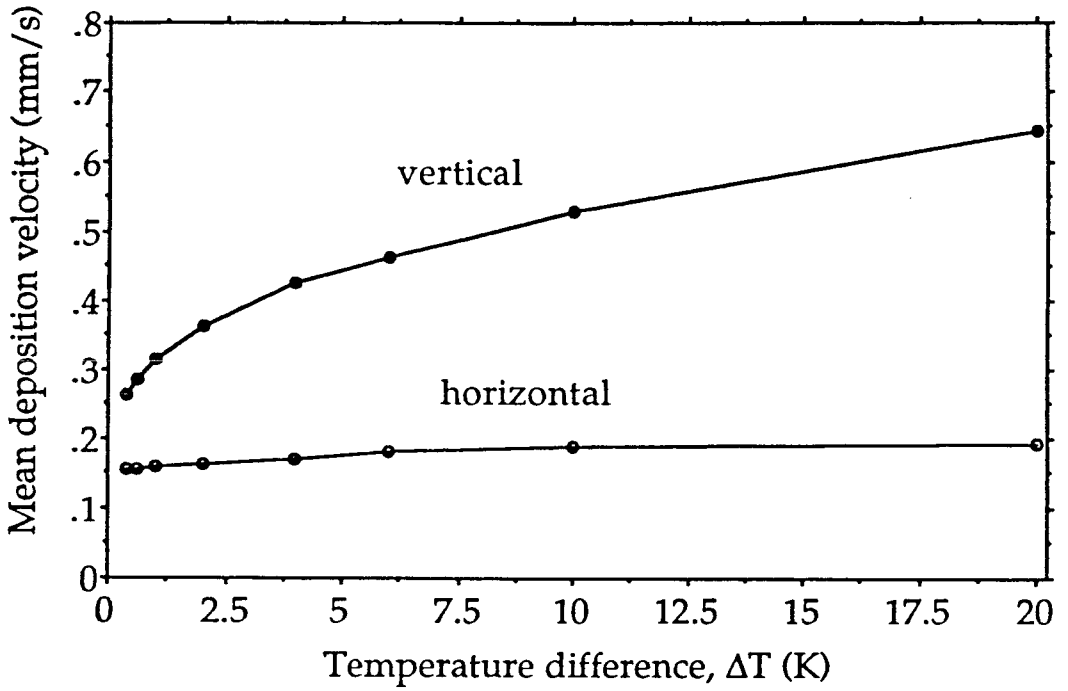

FIGURE 9. Mean deposition velocity of ^{218}Po over enclosure sides as a function of temperature difference, ΔT, for Case 1 geometry (see Figure 1). The diffusion coefficient is fixed at D = 0.056 $cm^2\ s^{-1}$, the enclosure dimension is fixed at H = 3 m, and the attachment rate is $\lambda_a = 0$. The problem was analyzed using a 29 × 29 grid.

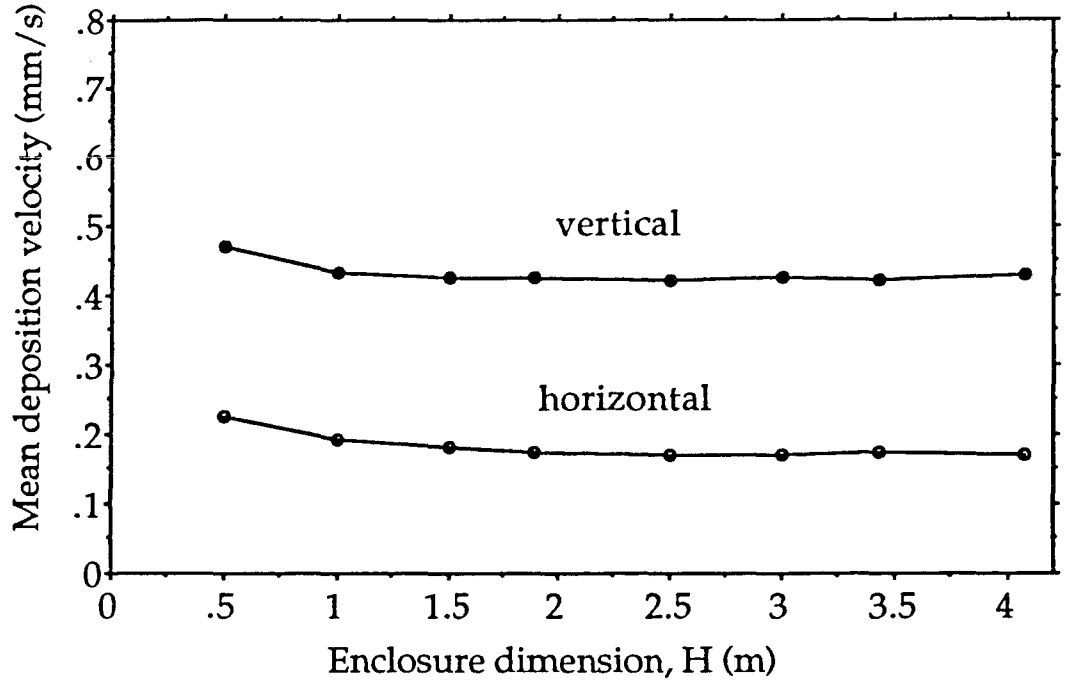

FIGURE 10. Mean deposition velocity of ^{218}Po over enclosure sides as a function of enclosure dimension, H, for Case 1 geometry (see Figure 1). The diffusion coefficient is fixed at D = 0.056 $cm^2\ s^{-1}$, the temperature difference between the vertical sides is fixed at $\Delta T = 4$ K, and the attachment rate is $\lambda_a = 0$. The problem was analyzed using a 29×29 grid.